Computer Methods and Programs in Biomedicine 151 (2017) 101–109

Contents lists available at ScienceDirect

Computer Methods and Programs in Biomedicine

journal homepage: www.elsevier.com/locate/cmpb

Combined endeavor of Neutrosophic Set and Chan-Vese model to extract accurate liver image from CT scan

Sangeeta K Siri[a], Mrityunjaya V. Latte[b]

[a] Department of Electronics & Communication Engineering, Sapthagiri College of Engineering, Bengaluru, karnataka 560057, India
[b] JSS Academy of Technical Education, Bengaluru, India

ARTICLE INFO

Article history:
Received 19 February 2017
Revised 29 June 2017
Accepted 22 August 2017

Keywords:
Neutrosophic Set
Chan-Vese model
Indeterminacy subset
Computed Tomography
Liver segmentation

ABSTRACT

Many different diseases can occur in the liver, including infections such as hepatitis, cirrhosis, cancer and over effect of medication or toxins. The foremost stage for computer-aided diagnosis of liver is the identification of liver region. Liver segmentation algorithms extract liver image from scan images which helps in virtual surgery simulation, speedup the diagnosis, accurate investigation and surgery planning. The existing liver segmentation algorithms try to extort exact liver image from abdominal Computed Tomography (CT) scan images. It is an open problem because of ambiguous boundaries, large variation in intensity distribution, variability of liver geometry from patient to patient and presence of noise. A novel approach is proposed to meet challenges in extracting the exact liver image from abdominal CT scan images. The proposed approach consists of three phases: (1) Pre-processing (2) CT scan image transformation to Neutrosophic Set (NS) and (3) Post-processing. In pre-processing, the noise is removed by median filter. The "new structure" is designed to transform a CT scan image into neutrosophic domain which is expressed using three membership subset: True subset (T), False subset (F) and Indeterminacy subset (I). This transform approximately extracts the liver image structure. In post processing phase, morphological operation is performed on indeterminacy subset (I) and apply Chan-Vese (C-V) model with detection of initial contour within liver without user intervention. This resulted in liver boundary identification with high accuracy. Experiments show that, the proposed method is effective, robust and comparable with existing algorithm for liver segmentation of CT scan images.

1. Introduction

The liver is a vital organ that has many roles in the body, including building proteins and blood clotting factors, manufacturing triglycerides and cholesterol, glycogen synthesis and bile production. The liver is the largest internal organ. Infections such as hepatitis, cirrhosis (scarring), cancer and over effect of medications are identified diseases within liver. The foremost stage for computer-aided diagnosis of liver is the identification of liver region. Liver segmentation algorithms extract liver image from scan images which helps in virtual surgery simulation, speedup the disease diagnosis, accurate investigation and surgery planning.

The liver segmentation from CT scan images has gained a lot of importance in medical image processing field because 1 in every 94 men and 1 in every 212 women born are susceptible to liver cancer in their life time [1,2]. Liver cancer is one of the most common diseases, with increasing morbidity and high mortality [3,4]. The Liver cancer treatment requires maximum radiation dose to the tumour and minimum toxicity to the surrounding healthy tissues. This is the major challenge in clinical practice [5,6]. Selective Internal Radiation Therapy (SIRT) with Yttrium-90 (Y-90) microspheres is an effective technique for liver-directed therapy [7]. SIRT dosimetry requires accurate determination of the relative functional tumour(s) volume(s) with respect to the anatomical volumes of the liver in order to estimate the necessary Y-90 microsphere dose [8,9]. Clinically, accurate liver volume determination is accomplished through tedious manual segmentation of the entire Computerized Tomography (CT) scan. A task is greatly dependent on the skill of the operator. Manual segmentation is time consuming. Thus many automatic or semiautomatic techniques are available for segmentation and determine the volume of the liver accurately. This facilitates the operational process from a physician's viewpoint.

Extracting liver from CT scan or MRI scan images is of prime importance. Considerable work has been done in extracting liver from CT scan or MRI scan images; so a general solution has remained as challenge. Failure in getting a reliable and accurate segmentation algorithm is due to (1) Neighbour organs of liver like

E-mail addresses: sangeeta_mk@rediffmail.com (S.K. Siri), mvlatte@rediffmail.com (M.V. Latte).

http://dx.doi.org/10.1016/j.cmpb.2017.08.020
0169-2607/

kidneys, heart, stomach, etc. have same intensity level. (2) There is no definite shape, weight, size, volume or texture for a liver. All these parameters are subjective. (3) Edges are weak (4) Presence of artifacts in MRI images or CT scan images. (5) Variability of liver geometry from patient to patient. (6) Large variation in pixel level range throughout the liver section as well as from patient to patient.

2. Related work

Chen et al. [10] designed Chan-Vese model for liver segmentation in which Gaussian function is used to find liver likelihood image from CT scan images and obtaining the liver boundary using Chan-Vese model. They have used morphological operation to improve the results. Song et al. [11] proposed an automatic liver boundary marking method which is based on an adaptive Fast Marching Method (FMM). The liver image is separated from CT scan by manually fixing pixel intensity between 50 and 200. Median filter is applied to reduce noise and liver image is enhanced by sigmoidal function. In this, the image is converted into binary and FMM is applied to find liver boundary accurately. Wu et al. [4] developed a novel method for automatic delineation of liver on CT volume images using supervoxel-based graph cuts. This method integrates histogram-based adaptive thresholding, Simple Linear Iterative Clustering (SLIC) and graph cuts algorithm. Mehrdad et al. [12] proposed random walker based framework. In this, liver dome is automatically detected based on location of the right lung lobe and rib caged area and liver is extracted utilising random walker method. Xiaowei et al. [13] introduced a multi-atlas segmentation approach with local decision fusion for fast automated liver (with/without abnormality) segmentation on Computational Tomography Angiography (CTA). Zheng et al. [14] designed a feature-learning-based random walk method for liver segmentation using CT images. Four texture features are extracted and then classified to determine the probability corresponding to the test images. In this, seed points on the original test image are automatically selected. Peng et al. [15] designed a novel multiregion-appearance based approach with graph cuts to delineate the liver surface and a geodesic distance based appearance selection scheme is introduced to utilize proper appearance constraint for each subregion. Platero et al. [16] proposed a new approach to segment liver from CT scan which is combination of low-level operations, an affine probabilistic atlas and a multiatlas-based segmentation. AlShaikhli et al. [17] presented a novel fully automatic algorithm for 3D liver segmentation in clinical 3D CT images based on Mahalanobis distance cost function using an active shape model implemented on MICCAI-SLiver07 achieving in an accurate results. Li et al. [18] developed liver segmentation using 3D-convolutional neural network and accuracy of initial segmentation is increased with graph cut algorithm and the previously learned probability map. Li et al. [19] developed a technique to detect the liver surface which includes construction of statistical shape model using the principal component analysis; Euclidean distance transformation is used to obtain a coarse position in a source image. And accurate detection of the liver is obtained using deformable graph cut method. Zheng et al. [20] designed a tree-like multiphase level set algorithm for segmentation, based on the Chan-Vese model to detect objects in an image. The algorithm is effective for images which have sub-objects in the region.

3. Neutrosophic Set (NS)

Neutrosophic Set (NS) was introduced by Smarandache [21]. In neutrosophic set theory, every event has not only a certain degree of the truth but also a falsity degree with indeterminacy. These parameters are considered independently from each other [21,22]. An entity {*S*} is considered with opposite {Anti-*S*} and neutrality {Neut-*S*}. The {Neut-*S*} and {Anti-*S*} are referred to as {Non-*S*} [22].

To apply the concept of NS to image processing, the image should be transformed into the neutrosophic domain. Image *P* of size *X***Y* with *K* grey levels can be defined as three arrays of neutrosophic images described by three membership sets: *T* (true subset), *I* (indeterminate subset) and *F*(false subset). Therefore, a pixel *P*(*i, j*) in the image transferred into the neutrosophic domain can be represented by $P_{NS}=\{T(i,j), I(i,j), F(i,j)\}$ or $P_{NS}=P(t,i,f)$. It means that the pixel is *% t* true, *% i* indeterminate and *% f* false. Here, t varies in T (white pixel set), i varies in I (noise pixel set) and f varies in F (black pixel set) which are defined as follows [21–24].

$$T(i,j)=\frac{\bar{G}(i,j)-\bar{G}_{min}}{\bar{G}_{max}-\bar{G}_{min}} \tag{1}$$

$$I(i,j)=\frac{d(i,j)-d_{min}}{d_{max}-d_{min}} \tag{2}$$

$$F(i,j)=1-T(i,j) \tag{3}$$

Where $\bar{G}(i,j)$ is local mean value of the pixel of the window and given by following equation

$$\bar{G}(i,j)=\frac{1}{w*w}\sum_{m=i-w/2}^{m=i+w/2}\sum_{n=i-w/2}^{j+w/2}G(m,n) \tag{4}$$

$d(i,j)$ is absolute value of the difference between intensity $G(i,j)$ and its local mean value $\bar{G}(i,j)$ and given as

$$d(i,j)=abs(G(i,j)-\bar{G}(i,j)) \tag{5}$$

$G(i,j)$ is intensity value of the pixel $P(i,j)$, w is size of sliding window, $\bar{G}_{min}$ and $\bar{G}_{max}$ are minimum and maximum of the local mean values of the image, respectively, d_{min} and d_{max} are minimum and maximum value of $d(i,j)$ in whole image.

4. Basic Chan-Vese model

All the classical snakes and active contour model depends on the image gradient to stop curve evolution, so these models can detect only objects with edges defined by gradient [25]. In biomedical images, edges are fragile and image is noisy. Hence stopping function is never zero on edges and the curve evolution may pass through the boundary. T.F. Chan and L.A. Vese have designed a new active contour model for image segmentation based on region instead of gradient, which is called Chan-Vese[C-V] model [26]. In this section, summary of original C-V approach [25] is presented for reader convenience.

Let $I(x)$ be the brightness function of input image. The image is defined over a two-dimensional area, denoted by $\Re$. It is assumed that, the image contains objects and background which have constant brightness, denoted by B_o and B_b respectively. Let C represents closed curve in the image that separates the objects and background. In C-V model [26], the following energy function is minimised.

$$\begin{aligned} f(B_o,B_b,C)=\mu\cdot Length(C)+\lambda\cdot Area(inside(C)) \\ +\lambda_o\int_{insideC}(I(x)-B_o)^2dx \\ +\lambda_b\int_{outsideC}(I(x)-B_b)^2dx \end{aligned} \tag{6}$$

Where λ_o,λ_b,μ, λ are parameters with suitably chosen values and are greater than or equal to zero. Eq. (6) can be minimised by taking function $\phi(x)$,$x\in\Re$, takes a value of greater than 0 inside the object, less than 0 outside the object and equal to zero on

boundaries. Heaviside function is used and is defined by

$$H(z) = \begin{cases} 1 & \text{if } z \geq 0 \\ 0 & \text{if } z < 0 \end{cases} \tag{7}$$

Applying Eq. (7), on Eq. (6)

$$f(B_o, B_b, \phi) = \mu \int_{\Re} |\nabla H(\phi)| dx + \lambda \int_{\Re} H(\phi) dx + \lambda_o \int_{\Re} (I - B_o)^2 H(\phi) dx + \lambda_o \int_{\Re} (I - B_o)^2 (1 - H(\phi)) dx \tag{8}$$

Keeping ϕ fixed and minimising the value of $f(B_o,B_b,C)$ with respect to the constants B_o,B_b. The expressions for B_o,B_b will be

$$B_o(\phi) = \frac{\int_{\Re} I \cdot H(x) dx}{\int_{\Re} H(x) dx} \qquad B_b(\phi) = \frac{\int_{\Re} I \cdot (1 - H(x)) dx}{\int_{\Re} (1 - H(x)) dx} \tag{9}$$

It can be easily seen that the values of $B_o(\phi)$ and $B_b(\phi)$ have the meaning of average brightness of original image over the areas that are regarded as objects ($\phi \geq 0$) and background ($\phi < 0$) respectively in image segmentation. Keeping B_o,B_b fixed and minimising $f(B_o,B_b,C)$ with respect to ϕ, the associated Euler–Langrange equation may be obtained as follows,

$$\delta(\phi)\left[\mu div\left(\frac{\nabla\phi}{|\nabla\phi|}\right) - \lambda - \lambda_o (I - B_o)^2 + \lambda_b (I - B_b)^2\right] = 0 \quad \text{in} \quad \Re \tag{10}$$

For practical computation, the author introduce regularization version of H and its derivation as follows

$$H_\varepsilon(z) = \frac{1}{2}\left(1 + \frac{2}{\pi} \arctan\left(\frac{z}{\varepsilon}\right)\right) \tag{11}$$

$\delta_\varepsilon(z) = H'_\varepsilon = \frac{1}{\pi} \cdot \frac{\varepsilon}{\varepsilon^2 + z^2}$ ε is suitably chosen value.

Introducing $\phi(T, x)$ by parameterizing the descent direction by time $T \geq 0$ and taking $\phi(0, x)$=$\phi_o(x)$ (chosen initial contour), a system is obtained for solving ϕ iteratively and can be written in the form of

$$\frac{d\phi}{dt} = \delta_\varepsilon(\phi)\left(\mu \cdot div\left(\frac{\nabla\phi}{|\nabla\phi|}\right) - \lambda - \lambda_o (I - B_o)^2 - \lambda_b (I - B_b)^2\right) \quad \text{in} \quad \Re \tag{12}$$

$$\phi(0, x) = \phi_o(x) \quad \text{in} \quad \Re \quad \text{and} \quad \left[\frac{\delta_\varepsilon(\phi)}{|\nabla\phi|} \frac{\partial \phi}{\partial \vec{n}}\right] = 0 \quad \text{on} \quad \Re$$

Where $\vec{n}$ denotes exterior normal to the boundary $\partial\Re$ of $\Re$ and $\frac{\partial\phi}{\partial\vec{n}}$ denotes normal derivation of ϕ at the boundary. $\phi_o(x)$ is a Signed Distance Function(SDF) and initial contour is defined as a curve satisfying $\phi_o(x) = 0$.

5. Methodology

5.1. Pre-processing phase

Abdominal CT scan image is with 1019×682 DICOM colour format. First convert the CT scan image into grey scale image of size 512×512. Reduce the noise using median filter.

5.2. Map the CT scan image into NS domain

Step1: Crop random section of liver image.

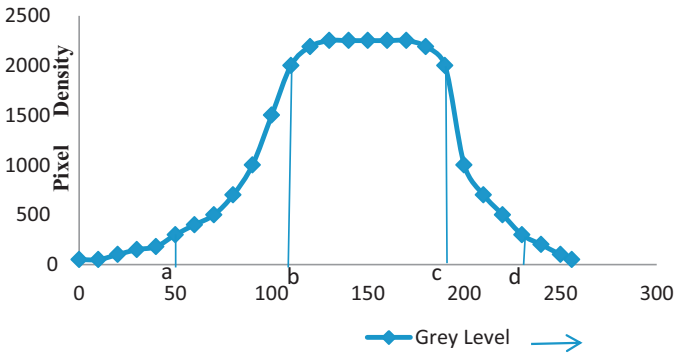

Fig. 1. Bell function.

Step2: Obtain *true subset T and false subset F* using bell function

$$T(x, y) = \pi(C_{xy}, a, b, c, d) \begin{cases} 0 & 0 \leq C_{xy} < a \\ \frac{(C_{xy} - a)^2}{(d-a)(d-a)} & a \leq C_{xy} < b \\ 1 - \frac{(C_{xy} - b)}{(d-c)(d-c)} & b \leq C_{xy} \leq c \\ \frac{(C_{xy} - d)^2}{(d-c)(d-c)} & c \leq C_{xy} \leq d \\ 0 & C_{xy} > d \end{cases} \tag{13}$$

$$F(x, y) = 1 - T(x, y) \tag{14}$$

Where C_{xy} is intensity value of pixel (i, j) in cropped image of liver. Variables a, b, c *and* d are parameters that determine the shape of *bell* function as shown in Fig 1.

Values of variables a, b, c *and* d are obtained using histogram-based method as follows:

(a) Obtain histogram of the cropped liver section.
(b) Find local maxima of the histogram

$$P_{max}(g_1), P_{max}(g_2), P_{max}(g_3) \ldots\ldots\ldots\ldots\ldots\ldots\ldots\ldots, P_{max}(g_n)$$

(c) Calculate mean of local maxima

$$\bar{P}_{max} = \frac{\sum_{i=1}^{n} P_{max}(g_i)}{n} \tag{15}$$

(d) Find peak values greater than mean of local maxima $\bar{P}_{max}$.

$b - initial\ peak\ value$

$c - final\ peak\ value$

(e) Find standard deviation (std.div) of cropped section of liver

$$std.div = \left(\frac{1}{n}\sum_{i=1}^{n} (x_i - \bar{x})^2\right)^{1/2} \tag{16}$$

where $\bar{x} = \frac{1}{n}\sum_{i=1}^{n} x_i$

(f) Find value of a and d as follows

$a = b - std.div$

$d = c + std.div$

Step3: Convert T and F into binary [27,28]

Tth and *Fth* are thresholds in *true subset* (T) and *false subset* (F) respectively. These are also required to obtain indeterminacy subset (I). A heuristic approach is used to find the thresholds in T and F.

(a) Select an initial threshold t_o in T.
(b) Separate T by using t_o and obtain two new groups of pixels: $T1$, $T2$.
(c) ($mu1$ and $mu2$ are the mean values of these two groups.)

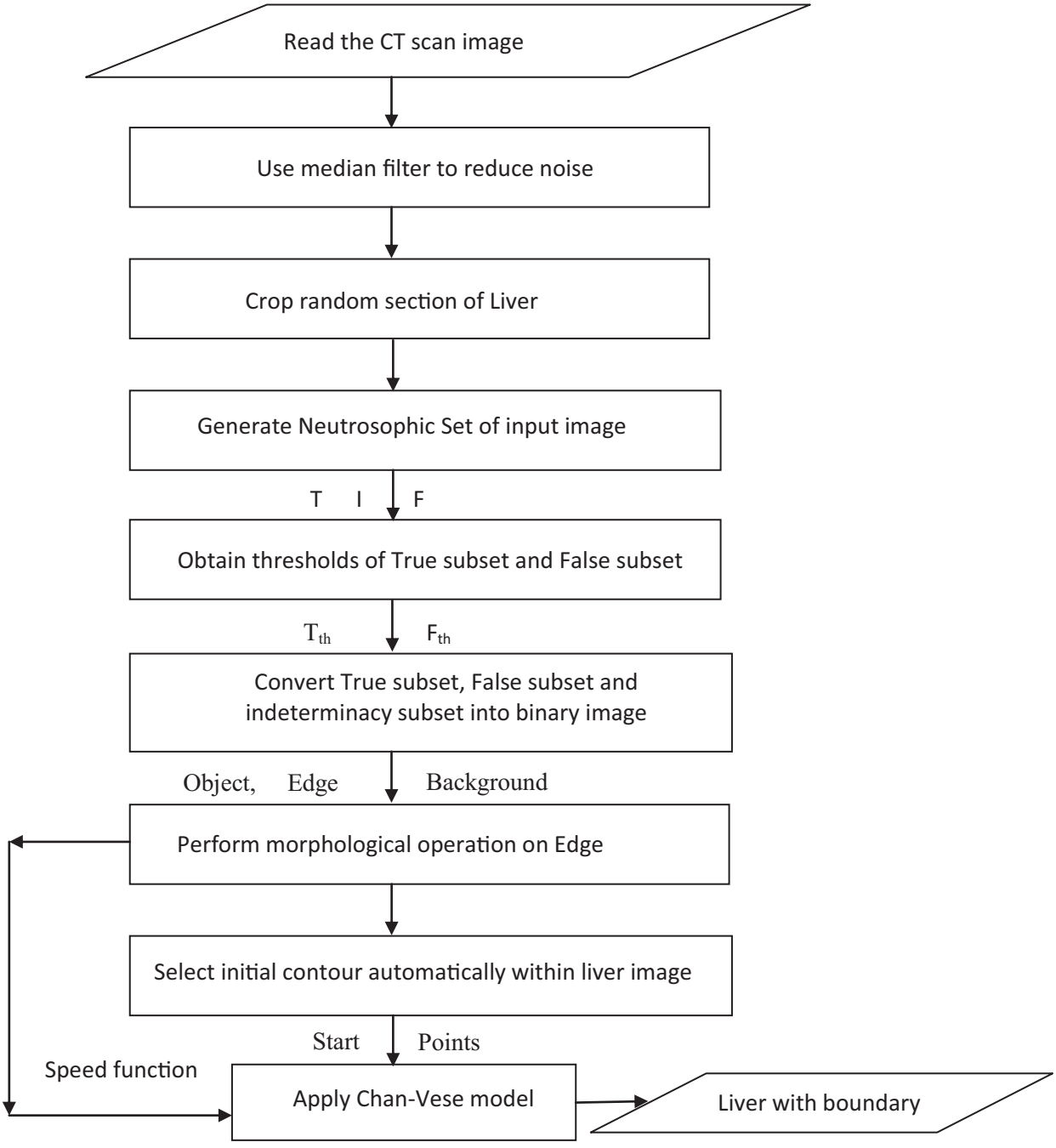

Fig. 2. Flowchart of the proposed method.

(d) Compute new threshold value $t_1 = \frac{mu1+mu2}{2}$

(e) Repeat step b through step d until the difference of $t_n - t_{n-1}$ is smaller than ε ($\varepsilon = 0.001$ in the experiment) in successive iterations. Then, threshold *Tth* is calculated by following substitution

$$Tth = t_n$$

(f) Above steps are repeated for finding *Fth* in *bset* (*F*) .

Step4: Find indeterminacy subset (*I*) [28]

Homogeneity is related to local information and plays an important role in image segmentation. We can define homogeneity by using the standard deviation and discontinuity of the intensity. Standard deviation describes the contrast within a local region, while discontinuity represents the changes in grey levels. Objects and background are more uniform and blurry edges are gradually changing from objects to background. The homogeneity value of objects and background is larger than that of the edges. A randomly identified size D X D window centered at (x, y) is used for computing the standard deviation of pixel (i, j):

$$S_d = \sqrt{\frac{\sum_{p=x-(D-1)/2}^{x+(D-1)/2} \sum_{q=y-(D-1)/2}^{y+((D-1)/2} (G_{xy} - mu_{xy})^2}{D^2}} \tag{17}$$

Where mu_{xy} is mean of intensity values within window and given by following equation

$$mu_{xy} = \frac{\sum_{p=x-(D-1)/2}^{x+(D-1)/2} \sum_{q=y-(D-1)/2}^{y+((D-1)/2} G_{xy}}{d^2} \tag{18}$$

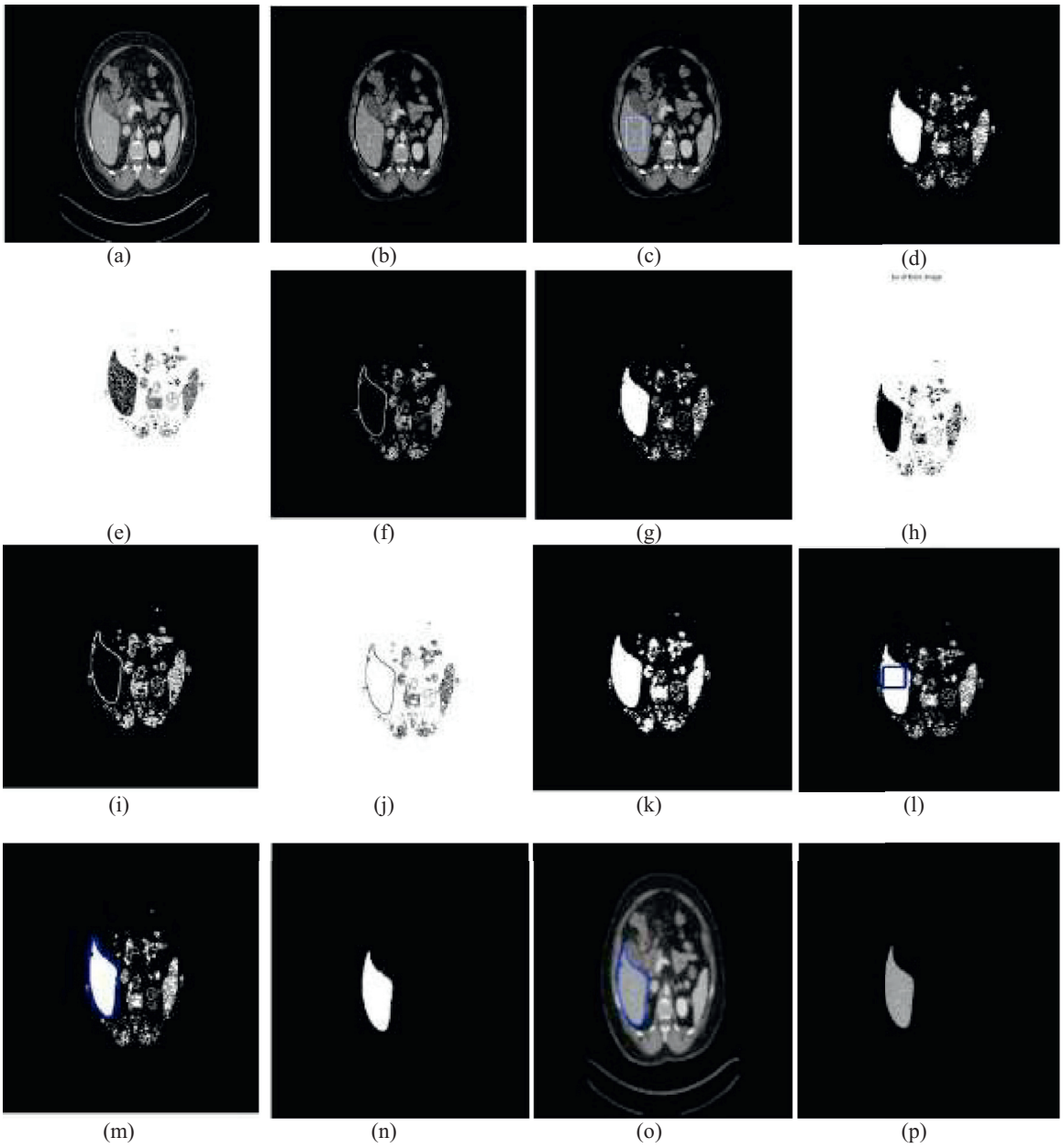

Fig. 3. (a) Original CT scan image; (b) Median filter image; (c) Cropping random section of liver;(d) True subset image; (e) False subset image; (f) Indeterminate image; (g) Foreground image; (h) Background image; (i) Edge image; (j) Homogeneity image; (k) Speed function; (l) Initial contour in speed function; (m) Liver boundary; (n) Extraction of liver from CT scan image; (o) Liver with boundary in CT scan; (p) Ground truth image.

The discontinuity of pixel $P(i,\ j)$ is described by the edge value. We use Sobel operator to calculate the discontinuity.

$$E_g(x,y) = \sqrt{{G_x}^2 + {G_y}^2} \tag{19}$$

Where G_x and G_y are horizontal and vertical derivative approximations.

Normalize the standard deviation, discontinuity and define the homogeneity as

$$H(x,y) = 1 - \frac{S_d(x,y)}{S_{dmax}} * \frac{E_g(x,y)}{E_{gmax}} \tag{20}$$

Where $S_{dmax} = \max\{S_d(x,y)\}$ and $E_{gmax} = \max\{E_g(x,y)\}$

The indeterminacy $I(x,\ y)$ is represented as

$$I(x,y) = 1 - \ H(x,y) \tag{21}$$

The value of $I(x,\ y)$ has a range of 0 to 1. The more uniform the region surrounding a pixel results in minimum value of the indeterminate pixel. The window size should be big enough to include enough local information, but still be less than the distance between two objects. We chose $D = 10$ in all calculations.

Step 5: Convert $T,\ F,\ and\ I$ into binary image:

(a) Procedure to find value of $\propto$

(a1) min = minimum{maximum values of each column in indeterminacy image $(I) \neq 0$}.

(a2) $\propto$ is any value less than or equal to min.

In this step, a given image is divided into three parts: object (Obj), edge(Edge) and Background (Bkg). $T(x,\ y)$ represents the degree of being an object pixel (Obj), $I(x,\ y)$ is the degree of being an edge pixel (Edge) and $F(x,\ y)$is the degree of being a background

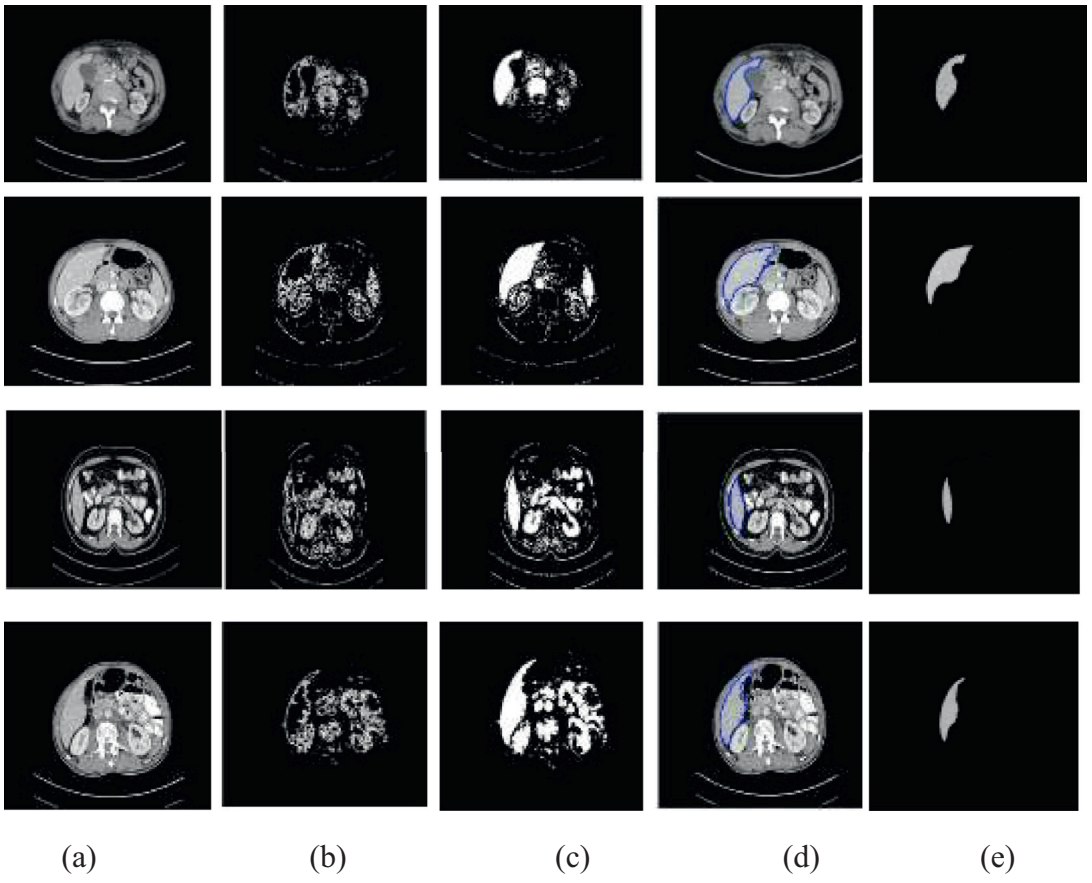

Fig. 4. Experimental results of proposed method.

pixel(Bkg) for pixel $P(x, y)$. The three parts are defined as follows:

$$Obj(x,y) = \begin{cases} True & T(x,y) \geq T_{th,} \quad I(x,y) < \propto \\ False & Others \end{cases} \tag{22}$$

$$Edge(x,y) = \begin{cases} True & T(x,y) < T_{th,} \vee F(x,y) < F_{th,} \quad I(x,y) \geq \propto \\ False & Others \end{cases} \tag{23}$$

$$Bkg(x,y) = \begin{cases} \text{True} & F(x,y) \geq F_{th,} I(x,y) < \propto \\ False & Others \end{cases} \tag{24}$$

The objects and background are mapped to 0 and the edges are mapped to 1 in the binary image. The mapping function is as follows

$$Binary(x,y) = \begin{cases} 0 & Obj(x,y) \vee Bkg(x,y) \vee \overline{Edge(x,y)} = \text{True} \\ 1 & \text{Others} \end{cases} \tag{25}$$

5.3. Post processing phase

Step 1: Perform morphological operation on indeterminacy set (I). This is called as speed function.

Step 2: Initial contour identification: Chan-Vese model requires an initial contour from which evolution of contour starts to detect the object boundary. In this paper, it is proposed, an effective initialization approach for segmentation of liver for Chan-Vese model. Following steps are designed.

(a) Find centroid of liver as$x_{cent}, y_{cent}, x_1 = 4, y_1 = 4$ and an area of liver.
(b) Take initial contour as (y_{cent},y_{cent}+y_1; x_{cent}, x_{cent}+x_1).
(c) Initialize stop=0.
(d) Let $\Omega \in R^2$ is a bounded domain. The Signed Distance Function (SDF) to Ω is function of R^2.

$x \in R^2$ and $x \mapsto \Phi_\Omega(x)$ is SDF defined by

$$\Phi_\Omega(x) = \begin{cases} -d(x,\partial\Omega) \; if \; x \in \Omega \; \; Interior - region \\ 0 \qquad\qquad if \, x \in \partial\Omega \; \; On - boundary \\ +d(x,\partial\Omega) \; if \; x \in \Omega^c \; Exterior - region \end{cases} \tag{26}$$

Where $d(\bullet,\partial\Omega)$ denotes the usual Euclidean distance function to the set $\partial\Omega$. $\partial\Omega$ represents boundary of an object.

(e) Generate the SDF from initial contour.
(f) Get narrow band of initial contour and find interior and exterior mean.
(g) Find the value of force using equation

$$F = (P-U)^2 + (P-V)^2 \tag{27}$$

Where U=interior mean, V=exterior mean and P=Pixel coordinate value

(h) If force (F) is less than 1 then increment x_1,y_1 value and go to step e else stop and take (y_{cent},y_{cent}+y_1; x_{cent}, x_{cent}+x_1) as initial contour.

Step3: Apply Chan-Vese model which detects liver boundary in CT scan.

The complete process of proposed technique is depicted in Fig 2.

6. Segmentation algorithm evaluation metric

In medical research, supervised evaluation is widely used [29]. It computes the difference between the reference image and the segmentation result using a given evaluation metric [30]. In this paper, the manual segmentation is adopted to reflect the reference image [31]. Evaluation of segmentation algorithms can be done by comparing the results obtained from algorithm-based segmented image against the same image being manually segmented by an expert. This is often referred to as ground truth or reference image [32]. The degree of similarity between the manually segmented image and machine segmented image reflect the accuracy of the segmented images [29,32]. The accuracy measure is computed as presented in Eq. (28).

$$Seg.\ Accuracy = \frac{ACP}{TP} \tag{28}$$

Where ACP = Number of Acceptably Classified Pixels in segmented region

TP = Totality of Pixels in machine segmented image.

If segmentation accuracy is 1 then it is concluded as perfect segmentation i.e. machine segmented image is same as that of ground truth image. As segmentation accuracy move away from 1 that shows degree of deviation in segmentation.

7. Experimental results

The experimental dataset contains 110 patient's CT scan images which are provided by M/S CT scan Centre, Hubli, Karnataka, India. Each slice of CT scan is a 1019×682 size colour image.

The original CT scan image, filtered image and cropping of random section of liver are shown in Fig 3(a), (b) and (c) respectively. True subset, false subset and indeterminacy subset are shown in Fig 3(d), (e) and (f) respectively. The object image, background image and edge images are shown in Fig 3(g), (h) and (i) respectively. Homogeneity image, speed function and initial contour within liver section are shown in Fig 3(j), (k) and (l) respectively. Final liver boundary at final iteration, extraction of liver from abdominal CT scan and boundary of liver in CT scan image are shown in Fig 3(m), (n) and (o) respectively. The ground truth image is shown in Fig 3(p). Fig 4 illustrates Experimental results of proposed method of 4 images, in column (a) Input image; (b) Edge image of liver image; (c) Speed function of liver image; (d) Liver with boundary in CT scan; (e) ground truth image.

8. Comparison with existing methods

In this section, the performance of the proposed method is compared with original Chan-Vese(C-V) model of Chan et al. [25] with specifications: mu = 0.1, number of iterations=170 and initial contour position = [330,310; 340,330].

"A level set method for image segmentation in the presence of intensity inhomogeneities with application to MRI", by Li et al. [33], have demonstrated the segmentation process. The analysis was performed on the CT scan image with following specifications: mu = 1.0, epsilon = 1.0, time step = 0.10, sigma = 4, initial contour position = [160,220;190,240], number of iterations = 10. This is called as Level Set evolution (LSE) model.

"Minimization of Region-Scalable Fitting Energy for Image Segmentation", by Li et al. [34], have demonstrated the segmentation process and the analysis was performed on the CT scan image with following specifications: Sigma = 3.0, epsilon = 1.0, mu = 1.0, time step = 0.1, lamda1 = 1.0, lamda2 = 1.0, number of iterations = 25, initial contour position = [160, 200; 180, 200]. This method is called as Region-Scalable Fitting (RSF) model.

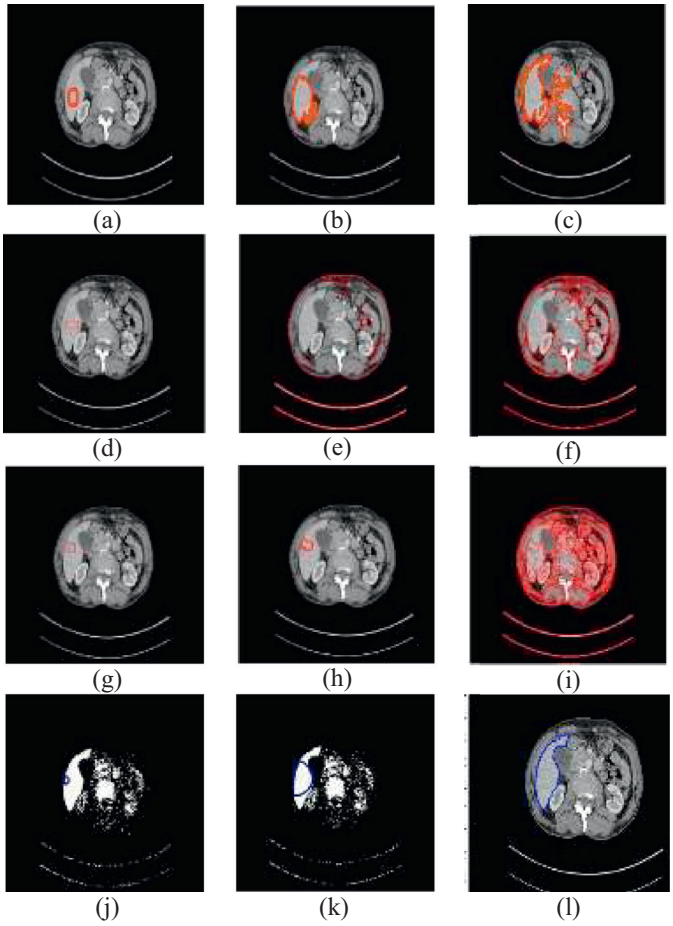

Fig. 5. (a), (d), (g), (j) show initial contour in the liver image for original Chan-Vese model, LSE model, RSF model and proposed method respectively; (b), (e), (h), (k) show intermediate results of original Chan-Vese model, LSE model, RSF model and proposed method respectively; (c), (f), (i), (l) show final segmentation results of original Chan-Vese model, LSE model, RSF model and proposed method respectively.

The initial contour in the liver section identified in C-V model; LSE model, RSF model and proposed method are shown in Fig 5(a), (d), (g) and (j) respectively. The intermediate results of C-V model, LSE model, RSF model and proposed method are shown in Fig 5(b), (e), (h) and (k) respectively. Final segmentation results of C-V model, LSE model, RSF model and proposed method are shown in Fig 5(c), (f), (i) and (l) respectively.

Liver and its neighbouring organs have same intensity level distribution, due to more noise and blurry edges, all three existing algorithms have limitations, resulting in inaccurate detection of exact liver section. The proposed methodology fully exploits the intensity distribution information by cropping random section of liver and its segmentation resulting in successful separation of liver image from its neighbouring organs.

In C-V model, LSE model and RSF model, it is necessary to identify initial contour and number of iterations manually. These parameters will affect the segmentation results. In the proposed method, there is no need to identify number of iterations and initial contour. Once complete liver boundary is detected, results will be displayed on computer screen. Initial contour is identified without user intervention.

The proposed algorithm, the original Chan-Vese (C-V) model, the LSE model and the RSF model have been tested for 110 images of CT scan. The average segmentation accuracy for original C-V model, LSE model, RSF model and the proposed model is listed in Table 1.

Table 1
Average Segmentation Accuracy for proposed model and existing algorithm.

	Original C-V model	LSE model	RSF model	Proposed model
Average Segmentation Accuracy	0.5228 ± 0.1655(SD)	0.4512± 0.1951(SD)	0.4030 ± 0.0.1807(SD)	0.9559 ± 0.0436(SD)

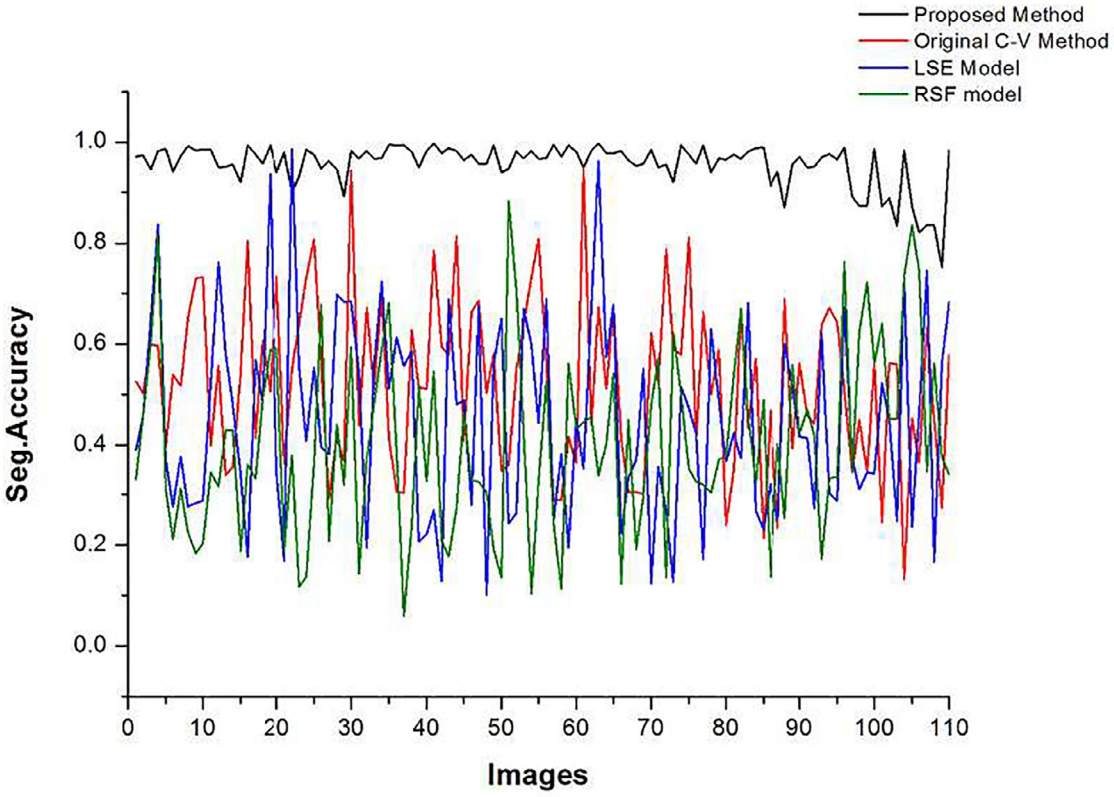

Fig 6. Comparison of the proposed method.

Where SD-Standard Deviation

On comparison of results, it is clear that, the accuracy is good and acceptable for all practical intervention of image analysis.

The proposed method has been simulated on processor specification of Intel(R), CPU T5670@1.8 GHz, 32bit operating system and RAM of 2.0GB with Matlab version of R2006a.

9. Discussions

The proposed design introduces a novel framework for liver segmentation from CT scan images, based on Neutrosophic Set (NS) and Chan-Vese model. A new scheme is designed to detect the initial contour within the liver section which is primary requirement of Chan-Vese model. The initial contour evolves outwardly to detect the exact liver boundary in CT scan image. The novel technique is proposed to convert an abdominal CT scan image to NS domain. NS domain gives an approximate structure of liver, which is verified and validated with practicing doctors. The results obtained are compared with ground truth images or reference images and it is observed that the contour identification is resulting in good acceptable accuracy. Fig 6 illustrates comparison of the proposed method.

10. Conclusions

Liver cancer treatment is complex and involves different actions, which include many times a surgical procedure. Medical imaging provides important information for surgical planning, and it usually demands an accurate liver segmentation from abdominal CT scan. This study proposes a methodology to segment the liver from abdominal CT scan images. A new scheme is proposed to transform an abdominal CT scan image into Neutrosophic domain which removes neighbouring structures of liver and provides an approximate structure of liver.

The new algorithm is designed to detect an initial contour within the liver which evolves superficially to detect boundary of liver using Chan-Vese model. This can be used for finding area and volume of liver which helps the physician diagnoses and liver transplantation. This can also be applied to detect other anatomical structures of abdomen like kidney, spleen, etc. with minor modifications. The proposed framework attains highest accuracy rate since it exploits intensity distribution information by cropping random section of liver.

Acknowledgement

The authors acknowledge the support of M/S Hubli Scan Center, Hubli, Karnataka, India and doctors working there for suggestions and certifications of results. The authors are thankful to the management and authorities of JSS Academy of Technical Education, Bengaluru, Karnataka, India and Sapthagiri College of Engineering, Bengaluru, Karnataka, India.

References

[1] American Cancer Society, Cancer Facts & Figures, USA: American Cancer Society, Atlanta, Ga, 2010.

[2] A. Jemal, F. Bray, M.M. Center, J. Ferlay, E. Ward, D. Forman, Global cancer statistics, CA Cancer J. Clinicians 61 (2) (2011) 69–90 [PubMed].
[3] J. Ferlay, I. Soerjomataram, R. Dikshit, et al., Cancer incidence and mortality worldwide: sources, methods and major patterns in GLOBOCAN 2012, Int. J. Cancer 136 (5) (2015) e359–e386.
[4] W. Wu, Z. Zhou, S. Wu, Y. Zhang, Automatic liver segmentation on volumetric CT images using supervoxel-based graph cuts, Comput. Math. Methods Med. 2016 (2016).
[5] R.S. Stubbs, R.J. Cannan, A.W. Mitchell, Selective internal radiation therapy with 90Yttrium microspheres for extensive colorectal liver metastases, J. Gastrointestinal Surg. 5 (3) (2001) 294–302 [PubMed].
[6] G.C. Pereira, M. Traughber, R.F. Muzic, The role of imaging in radiation therapy planning: past, present, and future, BioMed Res. Int. 2014 (9) (2014) 231090 [PMC free article] [PubMed].
[7] W.Y. Lau, S. Ho, T.W.T. Leung, et al., Selective internal radiation therapy for nonresectable hepatocellular carcinoma with intraarterial infusion of 90Yttrium microspheres, Int. J. Radiat. Oncol. Biol. Phys. 40 (3) (1998) 583–592 [PubMed].
[8] R. Murthy, R. Nunez, J. Szklaruk, et al., Yttrium-90 microsphere therapy for hepatic malignancy: devices, indications, technical considerations, and potential complications, Radiographics 25 (supplement 1) (2005) S41–S55 [PubMed].
[9] R. Bhatt, M. Adjouadi, M. Goryawala, S.A. Gulec, A.J. McGoron, An algorithm for PET tumor volume and activity quantification: Without specifying cameras point spread function (PSF), Med. Phys. 39 (7) (2012) 4187–4202 [PubMed].
[10] Y. Chen, Z. Wang, W. Zhao, Liver segmentation in CT images using Chan-Vese Model, The 1st International Conference on Information Science and Engineering (ICISE2009) 978-0-7695-3887-7/09.
[11] X. Song, M. Cheng, B. Wang, S. Huang, Automatic liver segmentation from CT images using adaptive fast marching method, Seventh International Conference on Image and Graphics. 978-0-7695-5050-3, IEEE, 2013 DOI -10.1109 /ICIG.2013.181.
[12] M. Mehrdad, et al., Automatic liver segmentation on computed tomography using random walkers for treatment planning, EXCLI J. 15 (2016) 500.
[13] X. Ding, et al., Fast automated liver delineation from computational tomography angiography, Procedia Comput. Sci. 90 (2016) 87–92.
[14] Y. Zheng, D. Ai, P. Zhang, Y. Gao, L. Xia, S. Du, X. Sang, J. Yang, Feature learning based random walk for liver segmentation, PLoS ONE 11 (11) (2016) 1–17.
[15] J. Peng, P. Hu, F. Lu, Z. Peng, D. Kong, H. Zhang, 3D liver segmentation using multiple region appearances and graph cuts, Med. Phys. 42 (12) (2015) 6840–6852.
[16] C. Platero, M.C. Tobar, A multiatlas segmentation using graph cuts with applications to liver segmentation in CT scans, Comput. Math. Methods Med. 2014 (2014) 16 Article ID 182909.
[17] S.D. Salman AlShaikhli, M.Y. Yang, B. Rosenhahn, 3D automatic liver segmentation using feature-constrained Mahalanobis distance in CT images, Biomedizinische Technik. Biomed Eng. 61 (4) (2015) 401–412 [PubMed].
[18] F. Lu, et al., Automatic 3D liver location and segmentation via convolution neural network and graph cut, Int. J. Comput. Assisted Radiol. Surg. 12 (2) (2017) 171–182.
[19] G. Li, et al., Automatic liver segmentation based on shape constraints and deformable graph cut in CT images, IEEE Trans. Image Process. 24 (12) (2015) 5315–5329.
[20] G. Zheng, H.-N. Wang, Y.-L. Li, A tree-like multiphase level set algorithm for image segmentation based on the Chan-Vese model, Dianzi Xuebao(Acta Electronica Sinica) 34 (8) (2006) 1508–1512.
[21] F. Samarandache, A Unifying Field in Logics Neutrosophic logic, in Neutrosophy. Neutrosophic Set, Neutrosophic Probability, third ed, American Research Press, 2003.
[22] Mohan J., Krishnaveni V. and Yanhui Huo, Automated brain tumor segmentation on mr images based on neutrosophic set approach, IEEE sponsored 2nd International Conference on Electronics and Communication System (icecs 2015).
[23] H. Abed, G. Maryam, R. Abdolreza, Scheme for unsupervised colour–texture image segmentation using neutrosophic set and non-subsampled contourlet transform, IET Image Process. 10 (6) (2016) 464–473 Iss.
[24] Y. Guo, H.D. Cheng, New neutrosophic approach to image segmentation, Pattern Recognit. 42 (5) (2009) 587–595.
[25] T. Chan, L.A. Vese, in: Active Contours Without Edges, IEEE Transactions On Image Processing, 10, IEEE inc, New York, 2001, pp. 266–277.
[26] J. Zhao, X. Zhang, W. Huang, F. Shao, Y. Xu, An improved Chan-Vese model without reinitialization for medical image segmentation, 2010 3rd International Congress on Image and Signal Processing, 2010.
[27] R.C. Gonzalez, R.E. Woods, Digital Image Processing, 3rd ed, Prentice Hall, 2007.
[28] M. Zhang, Novel approaches to image segmentation based on neutrosophic logic PHD Thesis, Utah item University, Logan, Utah, 2010.
[29] W. H. Elmasry, H.M. Moftah, N. El-Bendary and A. Ella Hassanien, Performance evaluation of computed tomography liver image segmentation approaches, 2012 12th International Conference on Hybrid Intelligent Systems (HIS).
[30] N. Situ, X. Yuan, G. Zouridakis, and N. Mullani, Automatic segmentation of skin lesion images using evolutionary strategy, In Proc. IEEE International Conference on Image Processing.
[31] X. Li, B. Aldridge, J. Rees, R. Fisher, Estimating the ground truth from multiple individual segmentations with application to skin lesion segmentation, in: Proc. 14th Annual Technical Meeting on Medical Image Understanding and Analysis (MIUA), Coventry, UK, University of Warwick, 2010.
[32] A.A. Betanzos, B. Arcay Varela, A. Castro Martnez, Analysis and evaluation of hard and fuzzy clustering segmentation techniques in burned patient images, Image and Vision Computing 18 (13) (2000) 1045–1054.
[33] C. Li, R. Huang, Z. Ding, J.C. Gatenby, D.N. Metaxas, J.C. Gore, A level set method for image segmentation in the presence of intensity inhomogeneities with application to MRI, IEEE Trans. Image Process. 20 (July(7)) (2011).
[34] C. Li, C.-Y. Kao, J.C. Gore, Z. Ding, Minimization of region-scalable fitting energy for image segmentation, Trans. Image Process. 17 (October(10)) (2008).